Robust Modeling of Tropospheric Delay Dynamics for Sequential Positioning

Elisa Gallon
Illinois Institute of Technology
Chicago IL, U.S.A.
egallon@hawk.iit.edu

Mathieu Joerger
Virginia Tech
Blacksburg VA, U.S.A.
joerger@vt.edu

Boris Pervan
Illinois Institute of Technology
Chicago IL, U.S.A.
pervan@iit.edu

***Abstract*— In this paper, we develop robust stochastic models of tropospheric delay accounting for uncertainty in residual tropospheric error time-correlation. This work is intended for time-sequential positioning and fault detection algorithms including, for example, integrated inertial navigation systems and dual-frequency, multi-constellation Advanced Receiver Autonomous Integrity Monitoring (ARAIM).**

I. INTRODUCTION

This paper describes time-domain and frequency-domain analyses of residual tropospheric delays. Months of experimental data from multiple globally distributed locations are leveraged to derive robust tropospheric error models for time-sequential navigation algorithms, including integrated inertial navigation systems and Advanced Receiver Autonomous Integrity Monitoring (ARAIM).

In the currently envisaged implementation of baseline ARAIM, carrier smoothed code (CSC) measurements at one instant in time are used to provide a 'snapshot' navigation solution (see [1], [2] and [3]). It was shown in [2] that baseline ARAIM cannot provide availability performance better than LPV-200, which has a 35 m Alert Limit (AL). In contrast, a time-sequential implementation of ARAIM using measurements collected over time can exploit satellite motion to significantly reduce Protection Levels (PL). Exploiting satellite motion will provide superior positioning performance and tighter PLs compared to baseline ARAIM [4]. By potentially achieving 10-meter ALs, sequential ARAIM algorithms (using batch estimators or Kalman filters) open the possibility to extend the scope of ARAIM applications beyond aircraft navigation, to rail, harbor, or arctic navigation. However, in time-sequential implementations, measurement error time-correlation must be modeled for all error sources including tropospheric delay, satellite clock and orbit ephemeris, and multipath. In prior work [5], satellite orbit and clock errors were characterized over time and their autocorrelation functions were upper and lower bounded. In this paper, we develop high-integrity models for the tropospheric delay over time.

Atmospheric errors constitute a major source of ranging error in GNSS. When a GNSS signal travels through the atmosphere, it can be delayed and/or refracted. In ARAIM, for example, ionospheric errors are removed using dual-frequency signals. However, tropospheric errors are not frequency-dependent and cannot be removed using the same method; the range error contribution in the zenith direction is on the order of 2.4 m [6]. The tropospheric error is made up of dry and wet components. The dry component is caused by dry gases present in the troposphere. Its effects vary with local temperature and pressure. These variations are predictable to a large extent and can, therefore, be modeled accurately. The wet component of the tropospheric delay caused by water vapor and condensed water depends on weather conditions and is less predictable.

In current implementations of GNSS Space-Based and Aircraft-Based Augmentation Systems tropospheric delay is modeled for a single satellite at a single epoch using estimates of the dry and wet components of the vertical tropospheric delay, multiplied by an elevation-dependent mapping function (i.e., obliquity factor, see [1], [2], [3]). This function is given by the Wide Area Augmentation System (WAAS) Minimum Operational Performance Standards (MOPS) [7] and is expressed as:

$$m(\theta_i) = \frac{1.001}{\sqrt{0.002001 + sin^2(\theta_i)}} \qquad (1)$$

where θ_i is the elevation of satellite *i*.

The standard deviation of the residual range error contribution in the zenith direction is specified to be no larger than 0.12 m (see [2], [3]). Reference [7] also suggests that the correlation of the tropospheric delay over time be modeled as a first-order Gauss Markov Random Process (GMRP) with a 30-minute time constant. However, no reference is provided to justify this choice of time constant and no guarantees are provided with regard to integrity.

In 2008, [8] analyzed tropospheric residuals to the NOAA model using 10 stations in North America. Using the least-squares method, they estimated the best fitting covariance function to the sample autocovariance function of the residuals and developed four different models. These models covered the time correlation of the tropospheric residuals but were not robust models and were limited to North America and to the NOAA model. In the rest of this paper, we develop a robust model for the tropospheric residuals using data from a worldwide network of stations.

II. Evaluation Of Tropospheric Model

To model the tropospheric residuals, tropospheric measurements were taken from a set of IGS (International GNSS Service) stations. This section describes the data sets considered and the tropospheric delay generation methods.

A. IGS tropospheric measurements

The IGS is comprised of over 200 self-funded agencies, universities, and research institutions. It provides high precision GPS satellite orbit estimates using a worldwide network of reference stations. Based on these estimates, IGS developed tropospheric products [9] available on a daily basis and at a 5-minute rate, with a 1-sigma accuracy of 4 mm. These products include tropospheric Zenith Path Delay (ZPD) estimates as well as their statistics. In this work, we derive residuals for the MOPS tropospheric model, and for the GPT2w model (GPT2w stands for Global Pressure and Temperature 2 wet).

B. Reference stations selection

The impact of the tropospheric delay on a GNSS signal depends on the day of the year, the receiver's position, and the satellite's elevation. We evaluate these errors over one year, at 20 worldwide receiver locations depicted in Fig. 1.

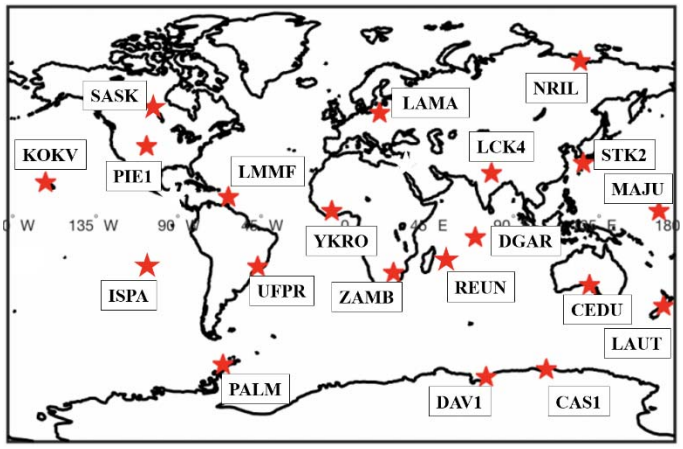

Fig. 1: IGS Reference Stations Distribution [10]

Note that three spatial stations are located in Antarctica and one in Russia to include extreme latitudes.

C. MOPS zenith tropospheric delay residuals

The total tropospheric zenith path delay and its error standard deviation are provided at each epoch in the IGS tropospheric files. The delay values are considered to be "truth" and are directly compared to the MOPS tropospheric model to obtain the tropospheric residuals, which are expressed as:

$$T_{res,MOPS} = \hat{T}_{MOPS} - T_{IGS} \qquad (2)$$

where:
T_{IGS} is the total tropospheric zenith path delay provided by IGS,
$\hat{T}_{MOPS}$ is the MOPS estimated zenith path delay.

In this work, we collected data spanning from the 1st of January to the 31st of December 2018 at 5 minute intervals for each of the 20 stations mentioned above. This represents a total of approximately two million data points. It is also important to note that we are focusing here on the zenith tropospheric delay, which is the only random part of the tropospheric residuals observed by a GNSS receiver (the mapping function being deterministic).

Table 1 summarizes the results obtained for each of the 20 stations. An emphasis is put on the stations DAV1, NRIL, CAS1, and PALM located at high latitude (Antarctica, Russia). These stations present the largest means even though their standard deviations remain small. On the other hand, stations located at low latitude (DGAR, YKRO, MAJU) have both small biases and standard deviations.

STATION	LAT. [deg]	LON. [deg]	MEAN [m]	STD [m]
LCK4	26.9	80.9	-0.092	0.122
STK2	43.5	141.8	-0.147	0.080
CEDU	-31.9	133.8	-0.142	0.044
DAV1	-68.6	78	-0.304	0.022
DGAR	-7.3	72.4	0.007	0.047
KOKV	22.1	-159.7	-0.042	0.046
PALM	-64.8	-64.1	-0.283	0.029
YKRO	6.9	-5.2	-0.027	0.062
MAJU	7.1	171.4	0.064	0.048
UFPR	-25.4	-49.2	-0.019	0.058
NRIL	69.4	88.4	-0.222	0.044
LAMA	53.9	20.7	-0.149	0.053
CAS1	-66.9	110.5	-0.316	0.027
SASK	52.2	-106.4	-0.155	0.043
REUN	-21.2	55.6	-0.041	0.048
PIE1	34.3	-108.1	-0.051	0.044
ZAMB	-15.4	28.3	-0.022	0.061
LAUT	-17.6	177.4	0.010	0.075
LMMF	14.6	-109.3	-0.036	0.048

Table 1: Statistics of MOPS tropospheric residuals for 20 reference stations

Fig. 2 presents these results in the form of error bars. The tropospheric residual for each of the 20 stations over year 2018 were gathered and arranged in 10-degree latitude bins. The mean and standard deviation of the binned residuals are represented in the figure. In addition, the number on top of the error bar indicates how many stations were included in each bin. This emphasizes again the fact that the MOPS tropospheric residual error distributions are strongly latitude dependent.

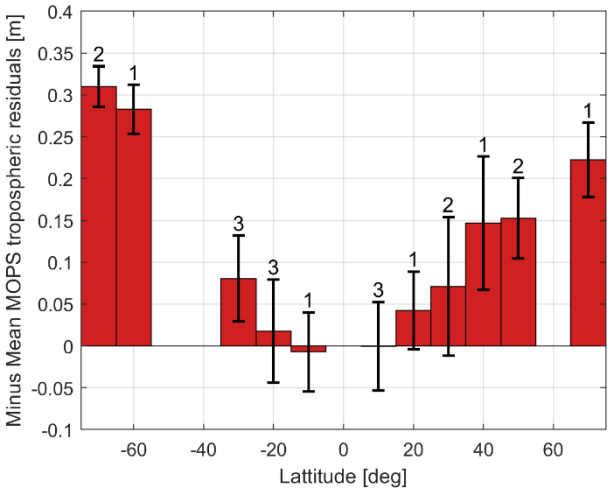

Fig. 2: MOPS Tropospheric residuals statistics over 20 reference stations

Weather, and humidity in particular, is expected to have a large impact on tropospheric errors. Fig. 3 shows tropospheric residuals at the KOKV station, which is located in the southeast of Hawaii. In August 2018, Hurricane Lane moved across the Hawaiian Islands and reached Category 5 on August 22 (Day of the Year - DoY 234). This was the wettest tropical cyclone on record in Hawaii with rainfall accumulations of up to 1,500 mm. It remained a Category 5 hurricane for 5 days before being downgraded to a tropical depression on August 28 (DoY 240) and dissipating the following day.

The upper plot in Fig. 3 represents the tropospheric residuals at KOKV between June 20 and 30, 2018. June was the driest month of the year at this location and is used here as a reference for "nominal" tropospheric conditions. The lower plot in Fig. 3 shows residuals from August 21 to 31, 2018, at the peak of Hurricane Lane's activity. On day 234, the first day of the hurricane, the residuals mean is shifted from -0.05m to 0.05m and stay around this value for the entire duration of the storm. When the storm ends on day 241, the residuals return to their initial mean of -0.05m.

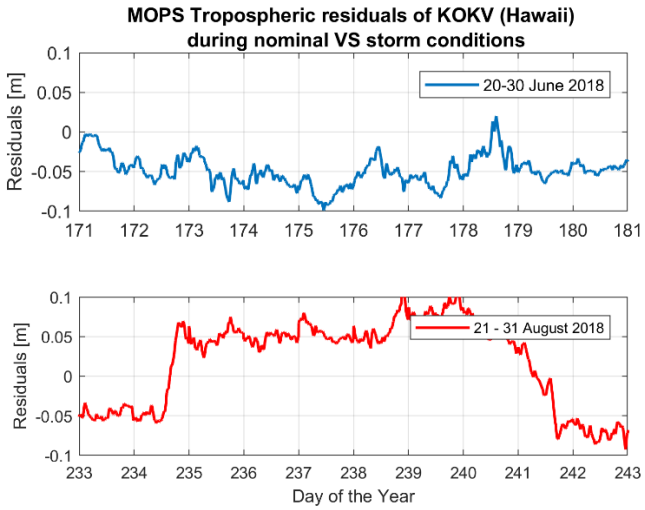

Fig. 3: Impact of a storm on MOPS tropospheric residuals

We note that extreme hurricanes as described above are rare and do not represent a large portion of weather events that an aircraft may encounter. However, an aircraft may fly over countries like India that are impacted by rainy seasons.

Fig. 4 represents the tropospheric residuals of station LCK4 located in the northeast part of India. This area is known for its intense rainy (monsoon) seasons. In this figure, the upper plot represents the tropospheric residuals during the month of January 2018 (driest month of 2018) and the lower plot represents those same residuals during the month of September 2018 (wettest month of 2018).

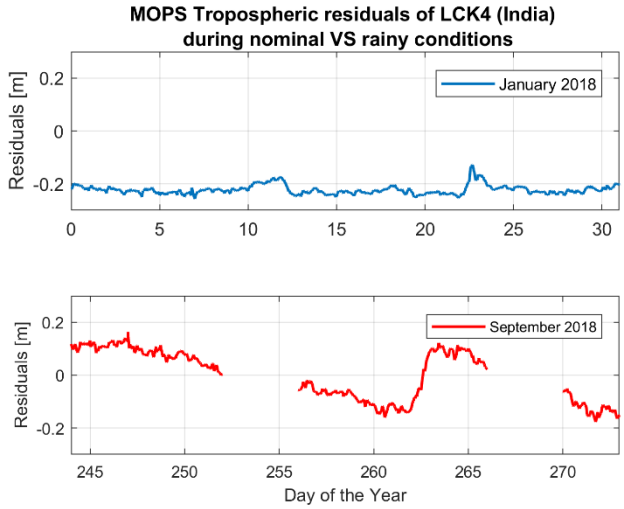

Fig. 4: Impact of the rainy season on MOPS tropospheric residuals

In contrast with the previous location (KOKV) where abrupt changes in weather conditions were observed, LCK4 is in an area that experiences slowly changing weather conditions. Note that the month of September is the end of the rainy season. This is consistent with the fact that, while the upper plot (dry season) shows constant residuals of -0.2 m, the lower plot varies, but slowly converges towards -0.2 m at the end of September.

Figure 2 shows that the MOPS model produces zenith tropospheric residuals that are biased by up to 30 cm at high latitude stations. The elevation mapping function in Equation (1) ranges from a value of 1 for a satellite at zenith to a factor of 10 for a low elevation satellite, so a low elevation satellite could be impacted by a 3 m bias. Biases this large may become dangerous for aircraft navigation. Thus, the MOPS model is best suited for low and mid latitude positioning. In the next subsection, we analyze the tropospheric residual errors using the more accurate GPT2w model.

D. GPT2w zenith tropospheric delay residuals

The GPT2w blind model is an empirical model of tropospheric delay developed in [11]. The term "blind" refers to the fact that no real time meteorological inputs are required. In this model, the wet delay is estimated using estimates of water vapor pressure, weighted mean temperature, and water vapor decrease factor. In our case, these values were provided in the form of a 1 deg by 1 deg latitude-longitude grid. This

grid is used to calculate pressure, temperature, temperature lapse rate, mean temperature of the water vapor, water vapor pressure, hydrostatic and wet mapping function coefficients, water vapor decrease factor, and geoid undulation for specific sites near the Earth surface. Using these data, the zenith hydrostatic delay is calculated using the refined Saastomoinen equation from [12] and the zenith wet delay is calculated using the method in [13]. Finally, the VMF1 (Vienna Mapping Functions 1) is used to compute the hydrostatic and wet mapping functions.

Unlike the MOPS model, which only takes the user latitude into consideration, the GPT2w model is a multi-dimensional grid tropospheric delay model using both latitude and longitude.

Using a similar approach to Section II.C, the GPT2w tropospheric residuals are computed as:

$$T_{res,GPT2w} = \hat{T}_{GPT2w} - T_{IGS} \quad (3)$$

where:

T_{IGS} is the total tropospheric zenith path delay provided by IGS,

$\hat{T}_{GPT2w}$ is the GPT2w estimated zenith path delay.

Residuals were processed for year 2018 using IGS data at a sampling rate of 5 minutes. Residuals were generated for all 20 stations.

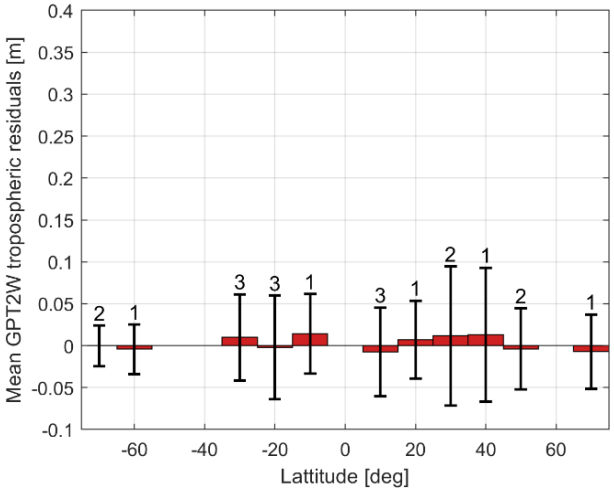

Fig. 5: GPT2W Tropospheric residuals statistics over 20 reference stations

Fig. 5 displays the mean and standard deviation of the GPT2w tropospheric residuals for various latitudes ranging from -70 to 70 deg. The numbers located above the error bars represent the number of stations used to compute the associated bar plot. In comparison to Fig. 2, the means of Fig. 5 are much lower (on the order of a few millimeters) but the standard deviations remain the same. This shows that the GPT2w model performs better than the MOPS model. This MOPS model's bias is shown in Fig. 2 to be dependent on the latitude of the receiver.

STATION	LAT. [deg]	LON. [deg]	MEAN [m]	STD [m]
LCK4	26.9	80.9	0.020	0.122
STK2	43.5	141.8	0.013	0.080
CEDU	-31.9	133.8	0.007	0.044
DAV1	-68.6	78	7.3e-4	0.022
DGAR	-7.3	72.4	0.014	0.047
KOKV	22.1	-159.7	0.007	0.046
PALM	-64.8	-64.1	-0.004	0.029
YKRO	6.9	-5.2	-0.057	0.062
MAJU	7.1	171.4	0.022	0.048
UFPR	-25.4	-49.2	0.013	0.058
NRIL	69.4	88.4	-0.007	0.044
LAMA	53.9	20.7	0.001	0.053
CAS1	-66.9	110.5	-0.001	0.027
SASK	52.2	-106.4	-0.009	0.043
REUN	-21.2	55.6	-0.001	0.048
PIE1	34.3	-108.1	0.003	0.044
ZAMB	-15.4	28.3	-0.004	0.061
LAUT	-17.6	177.4	-8.4e-4	0.075
LMMF	14.6	-109.3	0.012	0.048

Table 2: Statistics of GPT2W tropospheric residuals VS reference station

Table 2 provides more details on the GPT2w residuals for each station individually. In this case, the stations with the lowest mean values are stations DAV1 (Antarctica) and LAUT (Fiji) whereas the highest biases are observed at stations LCK4 (India), YKRO (Africa), and MAJU (Marshall Islands). The mean values of residuals do not vary significantly with receiver latitude.

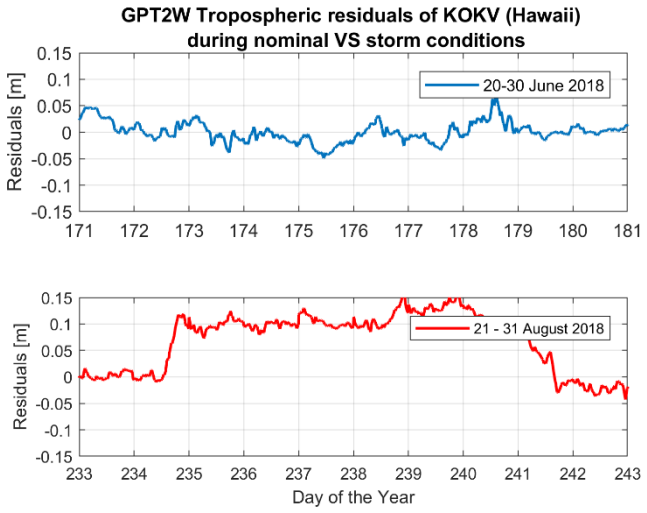

Fig. 6: Impact of a storm on GPT2w tropospheric residuals

Fig. 6 shows the tropospheric residuals of station KOKV in June (nominal conditions) and August 2018 (stormy conditions). Similar to the MOPS residuals, the GPT2w residuals change abruptly on DoY 234 (when the storm begins) and move back to normal on DoY 241 (end of the storm). This

observation confirms that neither MOPS nor GPT2w accurately model the tropospheric delay's behavior during an unexpected storm. This result was to be expected from Table 2 which showed that the standard deviations of MOPS and GPT2w residuals were similar. Fig. 6 appears to be a copy of Fig. 3 with mean residual values shifted towards zero during nominal conditions.

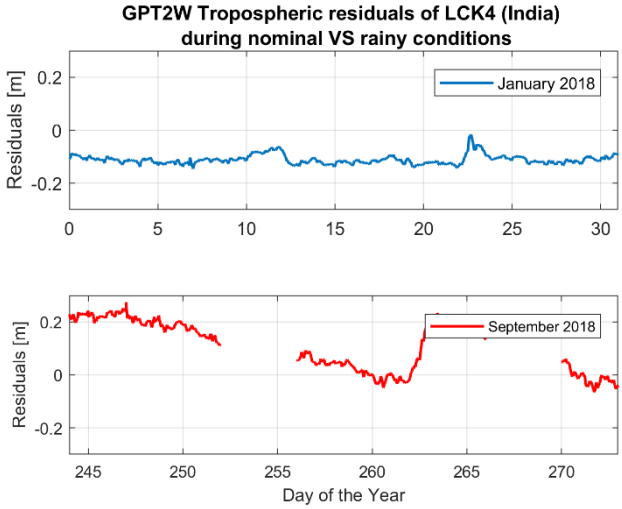

Fig. 7: Impact of the rainy season on GPT2W tropospheric residuals

Fig. 7 represents the tropospheric residuals of the station LCK4. GPT2w residuals have the same behavior as MOPS residuals under rainy and nominal conditions, but they are less biased (0.1 m) during nominal conditions.

E. Advantages and drawbacks of each model

The tropospheric model described in the MOPS documentation is derived from the UNB3 (University of New Brunswick) model [14]. The UNB3 model is a tropospheric delay model for use in aircraft that does not require meteorological parameters to be input in real-time. Instead, the UNB3 model relies on a 1D latitude-dependent lookup table. One of the main advantages of the MOPS model compared to the GPT2w model is that it requires low computational power. Because GPT2w requires the search of a 1 deg x 1 deg grid to estimate pressure, temperature, and water vapor information, it performs better but requires more computational power.

Implementing the GPT2w model in ARAIM would require changing the current RAIM processing algorithm. However, the switch from single-frequency RAIM to dual-frequency ARAIM may offer opportunities to also change the tropospheric model.

The results already presented show that humidity is impacting tropospheric residuals using both models. However, the GPT2w model was shown to perform much better than the MOPS model. The GPT2w residuals have biases on the order of millimeters and standard deviations on the order of centimeters. If we were to model the MOPS residuals as a random process, we would have to separate them into the sum of a GMRP and a constant bias. This bias was shown to be constant over time but dependent on the receiver's latitude. Another option to using GPTw directly would be to recalibrate the MOPS model biases using GPT2w. In Section III, we model the GPT2w error dynamics and take into account the prior observations by making sure that our error boundings cover these weather conditions. The residual errors of the MOPS and GPT2w differ only in the mean so their dynamics are the same.

III. Tropospheric Error Dynamics

In our prior work [5], orbit and clock errors were modeled by upper and lower bounding their autocorrelations. Using this approach for a time-sequential ARAIM implementation and combining it with the work in [15] will allow us to bound the integrity risk of our system. Therefore, the first part of this section will study the autocorrelation functions of the tropospheric residuals obtained for each of the 20 reference stations.

In [5], we also noted that the autocorrelation bounding approach has the advantage of being straightforward to implement (using the work in [15]). However, we also noted that this bounding was loose for short time intervals. In this work (Subsection III.B), we also present a new approach for error modeling: Power Spectral Density (PSD) bounding.

A. Tropospheric errors autocorrelation

Let us first look at the impact of the receiver's position (more specifically its latitude) on the tropospheric error correlation.

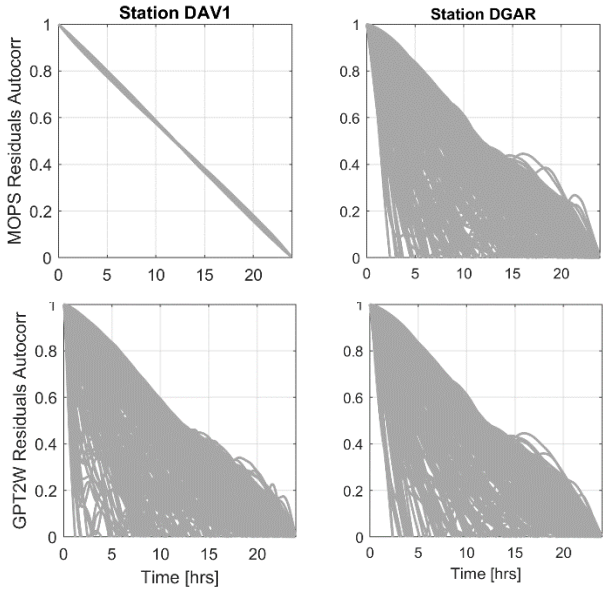

Fig. 8: Tropospheric residuals normalized autocorrelation for each day of 2018 at low (right) and high (left) latitudes

Fig. 8 shows the superimposed autocorrelation functions of each day of 2018 for the station DAV1 (located at high latitude) and DGAR (located at low latitude) using the MOPS residuals (upper figures) and GPT2w residuals (lower figures). Each of the indiviual autocorrelation functions were obtained using one day of data at a 5 minute sample (288 data points per day). For each station, 365×288 data points are plotted. The MOPS

residual autocorrelation functions confirm our previous remarks: High latitude stations have a larger bias and are less correlated than low latitude stations. In the following, we will be using the GPT2w residuals, which do not depend on the receiver's latitude. We can see that both low and high latitude station residuals have similar autocorrelation functions with the GPT2w residuals. They both show that the residual measurements are correlated. Trying to upper and lower bound these autocorrelations would result in loose bounds for any particular day, and hence conservative modeling. Instead, we will focus on another modeling method: upper bounding the Power Spectral Density (PSD).

B. *Tropospheric Error Power Spectral Density*

In the work of [15], unless the random process to be modeled is a first-order GMRP, integrity risk bounding via autocorrelation bounding is not a recursive method and requires continuous storing of the data (which is not possible in a KF). Modeling by bounding the PSD presents the advantage of being less restrictive, and more intuitive than autocorrelation bounding.

1) PSD estimation

When it comes to estimating power spectral densities, several methods exist [16]. In this work, we are limited to a discrete set of finite data. Hence, we will estimate PSD using the squared magnitude of the discrete Fourier transform (DFT) of our residuals.

In addition, note that any linear time-invariant operation on a function of time produces a new spectrum that will change the relative magnitude and/or phase of the frequency spectrum. In our case, using a finite, discretized data set (i.e., rectangular window input) and taking its FFT (Fast Fourier Transform) will produce a phenomenon called "sidelobe leakage." To account for this effect, the data values of each block will be tapered with a Hanning window [16].

The overall procedure is as follows:

- Divide the data into N contiguous blocks, each consisting of n values: $\{x_1, \dots, x_n\}$
- Apply the Hanning window u to reduce side-lobe leakage: $\{u.x_1, \dots, u.x_n\}$
- For each block, compute the N-point Fourier transform $X(f)$.
- Multiply it by a scale factor of $\sqrt{8/3}$, necessary to account for the loss due to tapering.
- Estimate the (two-sided) power spectral density of each block as follows:

$$\hat{S}_{xx_i}(f) = \frac{1}{n}|X_i(f)|^2, \quad i = 1, \dots, N \tag{4}$$

In the PSD estimation process, a recurrent dilemma arises between stationarity and PSD estimate accuracy. If short data sequences are used, the PSD estimate will most likely not be accurate (the FFT process may generate "fake" low frequency spikes). On the other hand, if long sequences are used, the process may not be stationary over the entire data set. The following subsection studies the tropospheric residuals stationarity in order to determine the amount of data required to estimate a PSD curve.

2) Stationarity analysis

In order to apply this procedure, one must first make sure that the data is stationary over the PSD estimation period (n days). In Fig. 9, tropospheric errors are presented over a period of 30 days for 4 different stations. The red dashed line represents a 7-day partitioning. The upper plot shows results for January (dry season – nominal conditions), and the lower plot for September (wet season). We can see that the process seems stationary over these 7-days windows of nominal conditions. Indeed, the residuals shown in this figure present slow variations, making it nonstationary over long period (e.g. 1 year), but when observed over short durations (e.g. 7 days), the process is stationary. In particular, we decided to not take longer periods than 7 days because, in the case of the monsoon season, 7 days is the maximum duration over which the process seemed stationary.

However, in Fig. 3, we observed that rare tropospheric events may occur, over short intervals of time (e.g., DoY 234), during which the process is not stationary anymore. These exceptions will be covered later as well as the monsoon cases covered before.

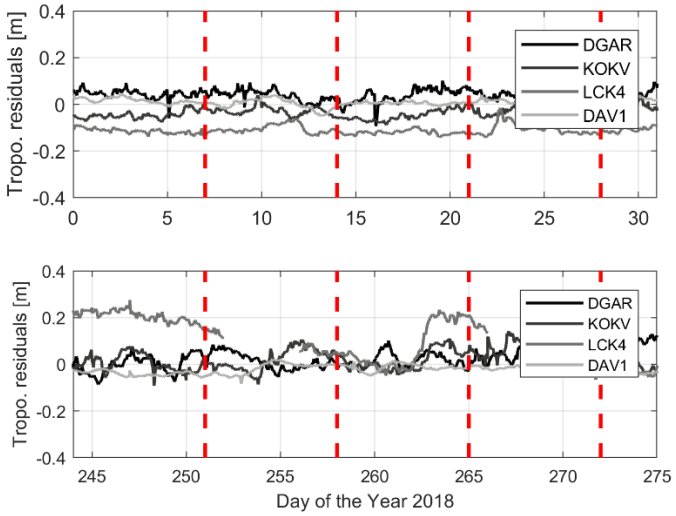

Fig. 9: Seven days partitioning of tropospheric residuals

In this work, we choose $n = 7$ days for the PSD estimation. Since we are using one year of data and partitioning it into 7-day blocks, we will end up with $N = 52$ curves per station, so a total of 52×20 PSD estimates covering the various receiver locations and weather conditions.

3) Power Spectral Density Bounding and Error Modeling

Fig. 10 represents the PSD of each of the 20 stations for the year 2018. As mentioned above, each PSD curve is obtained using 7 days of data. The red dashed curve represents the PSD of a first-order GMRP with time constant 110 min and standard deviation of 0.4m.

Clearly, this standard deviation value is much lower than the ones observed in Table 2. We can therefore conclude that the PSD obtained with real data do not match the PSDs of a first-order GMRP, regardless of our choice of time constant and standard deviation. As an alternative, the black curve represents

the PSD obtained with the following second-order transfer function:

$$H(s) = K\frac{\tau s + 1}{s^2} \quad (5)$$

where:

$K = 10^{-6}$ sec^{-2} and $\tau = 10$ sec

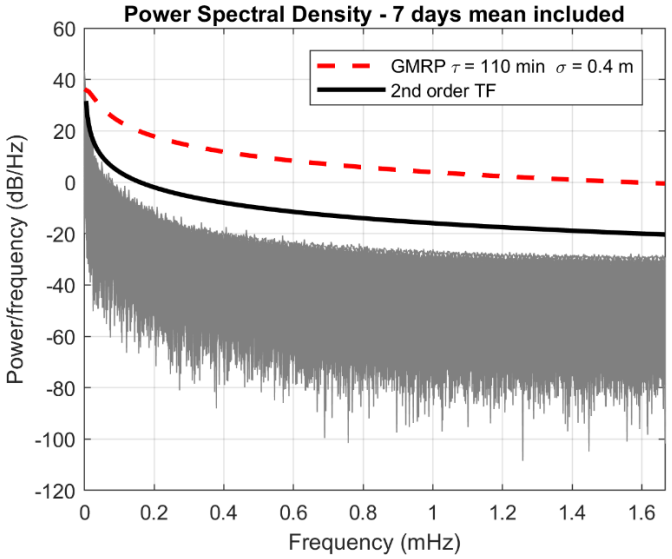

Fig. 10: GPT2w Tropospheric residuals Power Spectral Density bounding

Because a large amount of data (spanning through 2018 and covering various latitudes and weather conditions) was used to generate these PSD curves, we are confident that the PSD bounding presented here is conservative. However, Section II.D showed that the tropospheric residuals are not always stationary over 7 days. The following subsection covers these cases.

4) Non-stationary cases

In Fig. 3, we have observed sharp changes in the tropospheric residual when the station encountered a storm. We noted that the residuals were stationary before and after these sharp changes (DoY 234 and 241). Similarly, in Fig. 4 we observed that the process was not stationary at the onset monsoon season. In other words, only the transitions from no-storm to storm and no-monsoon to monsoon are nonstationary, the rest of the residuals are considered stationary over any 7-days period.

In future work, we will have to define a storm detector (using the Innovation of the KF) in order to detect storm fronts in real time, and switch to the appropriate dynamic model. When a storm will be detected, the algorithm will have to reset the tropospheric residual estimator.

5) Robustness of the model

In control theory, a model is said to be robust if the system can perform properly even if the dynamic model is not precisely known. In our case, this means that our predicted estimate error covariances will bound the actual estimate errors under all environmental conditions. To ensure that our model was robust, we decided to upper bound the PSDs obtained over many locations over a year, covering all sorts of weather conditions. In a future paper, we will provide the analytical proof that bounding the PSD provides a robust model.

IV. Conclusion

During 2018, the tropospheric residuals to the MOPS model showed a 30 cm bias for stations located at latitudes of approximately $\pm$ 65 degrees, compared to biases below 5 cm for stations located at latitudes between $\pm$ 20 degrees in latitude. The GPT2w tropospheric residuals, on the other hand, showed no dependencies on the receiver's latitude, and had an average observed bias of 1.5 cm over the 20 IGS stations selected for this work. The MOPS and GPT2w residuals had similar standard deviations of 5 cm on average.

During a Hawaiian storm in August 2018, the tropospheric residuals showed sharp/extreme variations which shifted the mean of the residuals by 10 cm for the entire duration of the storm, before dropping back near zero when the storm was over. During the rainy seasons in India however, the changes in tropospheric residuals were slower, but still reached up to 20 cm, before slowly coming back near zero at the end of the rainy season. Hence, both models were unable to predict the tropospheric delay during storm and rainy seasons, but GPT2w provides overall smaller residuals. We therefore recommend the use of GPT2w over the current MOPS model.

Finally, to model the tropospheric residuals dynamics, we have chosen PSD bounding over autocorrelation bounding. The PSDs of the 20 stations over 2018 could not be accurately bounded by a first order Gauss Markov Process. Instead the residuals dynamics was bounded using a second order transfer function.

V. Future Work

This paper showed that the GPT2w model presented smaller residual means and similar residuals standard deviations to the MOPS model. Since the GPT2w is more computationally expensive than the MOPS algorithm, we will calibrate the mean residuals differences between GPT2w and MOPS and store them in a latitude-dependent table. The user will simply have to use the computationally inexpensive MOPS model and correct it with the latitude-dependent table in order to obtain residuals in the order of cm.

Further analytical work will need to be performed to prove that PSD bounding provides a robust model of the tropospheric error dynamics. Additionally, this model and the model developed in [5] (provided it is refined to cover PSD bounding) can be used to assess the performance of a time sequential version of ARAIM. The integrity risk of this algorithm will then be derived from the work in [15].

Acknowledgment

The authors would like to thank the Federal Aviation Administration (FAA) for their support of this research.

However, the opinions in this paper are our own and do not necessarily represent those of any other person or organization.

REFERENCES

[1] Working Group C, "ARAIM Technical Subgroup. Interim Report Issue 1.0," Technical report, EU-US Cooperation on Satellite Navigation, 2012.

[2] Working Group C, "ARAIM Technical Subgroup. Milestone 2.0 Report," Technical report, EU-US Cooperation on Satellite Navigation, 2014.

[3] Working Group C, "ARAIM Technical Subgroup. Milestone 3.0 Report," Technical report, EU-US Cooperation on Satellite Navigation, 2016.

[4] M. Joerger and B. Pervan, "Multi-Constellation ARAIM Exploiting Satellite Geometry Change," in *Proceedings of the 28th International Technical Meeting of the Satellite Division of the Institute of Navigation (ION GNSS+)*, Tampa, FL, 2015.

[5] E. Gallon, M. Joerger, S. Perea and B. Pervan, "Error Modeling Development for ARAIM Exploiting Satellite Motion," in *Proceedings of Institute of Navigation (ION) GNSS+*, Miami, FL, 2019.

[6] J. Haase, M. Ge, H. Vedel and E. Calais, "Accuracy and Variability of GPS Tropospheric Delay Measurements of Water Vapor in the Western Mediterranean," *Journal of Applied Meteorology,* pp. 1547-1568, 2003.

[7] RTCA, "Minimum Operational Performance Standards for Global Positioning System/Wide Area Augmentation System Airborne Equipment system, RTCA DO-229E," 2016.

[8] H. E. Ibrahim and A. El-Rabbany, "A Regional Stochastic Model for NOAA-Based Residual Tropospheric Delay," in *ION NTM*, San Diego, CA, 2008.

[9] NASA CDDIS, "Troposphere solution directory," [Online]. Available: ftp://cddis.nasa.gov/gnss/products/troposphere/zpd/.

[10] J. Patel, Y. Zhai, S. Kiarash and S. Khanafseh, "Prototyping an ARAIM Offline Ground Monitor Using Experimental Data," in *Proceedings of Institute of Navigation GNSS+ Conference*, Miami, FL, 2018.

[11] J. Boehm, G. Moller, M. Schindelegger, G. Pain and R. Weber, "Development of an improved empirical model for slant delays in the troposphere (GPT2w)," *GPS Solut.,* vol. 19, no. doi: 10.1007/s10291-014-0403-7, pp. 433-441, 2014.

[12] J. L. Davis, T. A. Herring, A. E. E. Rogers and G. Elgered, "Geodesy by radio interferometry: Effects of atmospheric modeling errors on estimates of baseline length," vol. 20, pp. 1593-1607, 1985.

[13] J. Askne and H. Nordius, "Estimation of tropospheric delay for microwaves from surface weather data," *Radio Sci,* vol. 22(3), pp. 379-386.

[14] R. F. Leandro, M. C. Santos and R. B. Langley, "A North America Wide Area Neutral Atmoshpere Model for GNSS Applications," *NAVIGATION: Journal of The Institute of Navigation,* vol. 56, pp. 57-71, 2009.

[15] S. Langel, "Bonding Estimation Integrity Risk for Linear Systems With Structured Stochastic Modeling Uncertainty," PhD Dissertation, 2014.

[16] J. S. Bendat and A. G. Piersol, Random Data Analysis and Measurement Procedures, New Jersey: John Wiley & Sons, Inc., Hoboken, 2010.